Ferromagnetic Tridisk-Coupled Resonator and Magnetically Tunable Stripline Y Circulator

Tsukasa Nagao, *Senior Member, IEEE,* and Zengo Tanaka

Abstract—**A ferromagnetic tridisk-coupled (TDC) resonator was constructed by placing three YIG ferrite disks mutually attached on the circular center conductor. The EM fields in one of three disks is described in terms of expanded circular harmonics with an approximated transformation of derivative, and the EM fields in a TDC resonator is synthesized from the respective constituent EM fields of three disks, by sum-transformation, regarding three eigen junctures of the TDC resonator. The synthetic EM fields include coefficients A, B and D which are described as functions of radisu ratio r_0/r and azimuthal angle ϕ. In this paper, a special case that $A = D = 0$ is treated. It is remarked that the resonant mode curves having a lowered eigenvalue is bounded by the ferrite anisotropic splitting factor $B_0(\kappa/\mu)$, B_0 being a function of r_0/r_2 and $\phi = 0$. Calculation of two conditional equations of perfect Y circulation is carried out. Theoretical analysis of the magnetically tunable operation is made on the first conditional curves which are drawn superimposed on the resonant mode curves, and subsequently on the second conditional curves of Z_{ye} the equivalent input impedance of the stripline Y junction. The latter gives the graphical way of impedance matching of the devise.**

Finally the magnetically tunable operation is examined experimentally with the theoretical analysis.

Keywords—**Tridisk-coupled (TDC) resonator, expanded circular harmonics, eigen juncture, sum-transformation, synthetic electromagnetic (EM) fields, resonant mode, circulating mode, impedance adjustment, magnetically tunable operation.**

I. Introduction

As IS well known, most of stripline Y circulators have ever been made of single ferrite disk resonators, and a number of resonant modes existing in the resonator naturally takes part in circulator operation [1]–[3]. So it was thought that if a circulator was made of TDC resonators, since it was made of three ferrite disks joined together, at least three times more resonant modes than those in a single disk resonator might be excited and perhaps deteriorate stable operation as they interfere with each other. Experiments which we carried out, however, demonstrated that a stripline Y junction with TDC resonators achieved such a magnetically tunble operation in the above-resonance region [4].

As far as the authors are aware, no paper has been given to such TDC resonator and its applied circulator, but an analogy of a TDC resonator, if one consciously sees an optical fiber with multiple cores in its transverse section, may be found in literatures [5] and [6]. Their treatments of guiding wave modes are commonly designated as applying the continuity condition of EM fields to boundary surfaces of constituent fiber cores. They are considered directly unapplicable to analysis of TDC resonator, because in a TDC resonator EM fields outside the ferrite disks do not appreciably contribute to coupled modes of the resonator.

This paper aims, first, to analyze approximately coupled EM modes in the TDC resonator and, next, to explain the experimental results of a stripline Y circulator with TDC resonators which were recently reported elsewhere [4]. The method used is primarily based on an approximate transformation of variables in order to obtain the EM fields in constituent ferrite disks in terms of expanded circular harmonics. The EM fields in a TDC resonator are synthesized by joining the respective EM field components of three disks. The resonant modes are assumed to be determined by the boundary condition of the magnetically short circuited edge that applies to a circular periphery of the TDC resonator, the radius of which is adjusted, in the end, to the experimental value.

The synthesized magnetic fields and resonant modal characteristic equations include structural coefficients A, B and D which are functions of inverse radius ratio r_0/r and azimuthal angle ϕ, but in this paper only a special case that $A = D = 0$ is taken in II. To theoretically analyze the magnetically tunable operation in III, computed results of two conditional equations of perfect Y circulation with TDC resonators are utilized. With emphasis on impedance matching as circulation adjustment, the second circulation condition is contrived to get more understandable expression as input impedance of stripline Y junction. Experiments and discussions are presented in IV.

II. Theoretical Analysis of TDC Resonator

A. Circular Harmonic Expansion of The EM Fields

A TDC resonator is made of three ferrite disks mutually attached. Each ferrite disk is paced at an eccentric position of rotational symmetry allocated by $2\pi/3$ in circular center conductor as shown in Fig. 1. The biasing magnetic field is applied parallel to the common axis z. The dimensions of the resonator are such that the diameter of each constituent disk is 2a, its thickness t, the distance of

Manuscript received March 4, 1991, revised February 19, 1992.

The authors are with the Department of Electrical Engineering, National Defense Academy, Hashirimizu, Yokosuka, Kanagawa, 239 Japan.

IEEE Log Number 9201721.

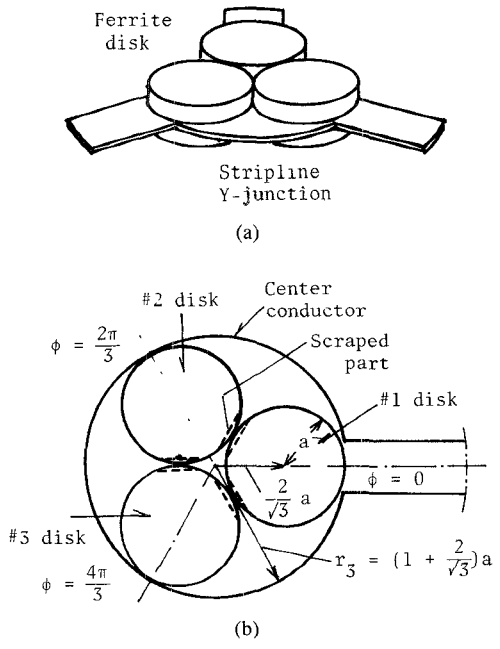

Fig. 1. (a) The stripline Y junction with TDC resonators, and (b) a geometrical configuration of the TDC resonator.

eccentricity r_0 which equals the distance $\overline{OQ}$, and the radius of the center conductor r_3 $(= (1 + 2/\sqrt{3})a)$.

As previously noted, the EM fields in a TDC resonator can be synthesized from those for three constituent ferrite disks which are positioned mutually attached symmetrically. Derivation of the EM fields in an eccentrically positioned disk resonator can be worked out, first, in converting the well known EM fields in a ferrite disk resonator into those harmonic components of an eccentrically positioned disk resonator, by help of addition theorem of Bessel functions (see Appendix A). Next, we sum up the respective EM fields of three eccentrically positioned disk resonators to get the EM fields in the TDC resonator.

Now we introduce a circular cylindrical coordinate system (r, ϕ, z) that applies to an eccentrically positioned ferrite disk centered at Q $(r_0, 0, z)$, and the other coordinates (ρ, θ, z) which only applies to a ferrite disk as shown in Fig. 2(a). With regard to a triangle ΔOPQ, it holds

$$\rho^2 = r^2 + r_0^2 - 2rr_0 \cos \phi, \tag{1}$$

$$\theta = \phi + \psi, \tag{2}$$

$$\rho \cos \psi = r - r_0 \cos \phi, \quad \rho \sin \psi = r_0 \sin \phi. \tag{3}$$

If we adopt new variables

$$w = k\rho, \quad Z = kr, \quad Z_0 = kr_0, \tag{4}$$

then (1) and (3) become

$$w^2 = Z^2 + Z_0^2 - 2ZZ_0 \cos \phi, \tag{5}$$

$$w \cos \psi = Z - Z_0 \cos \phi, \quad w \sin \psi = Z_0 \sin \phi, \tag{6}$$

and thereby we have two new coordinate systems (w, θ, z) and (Z, ϕ, z) instead of (ρ, θ, z) and (r, ϕ, z).

The EM fields in a circular ferrite disk resonator which is magnetized in the z direction are described in the circular cylindrical coordinates (ρ, θ, z) as follows [1],

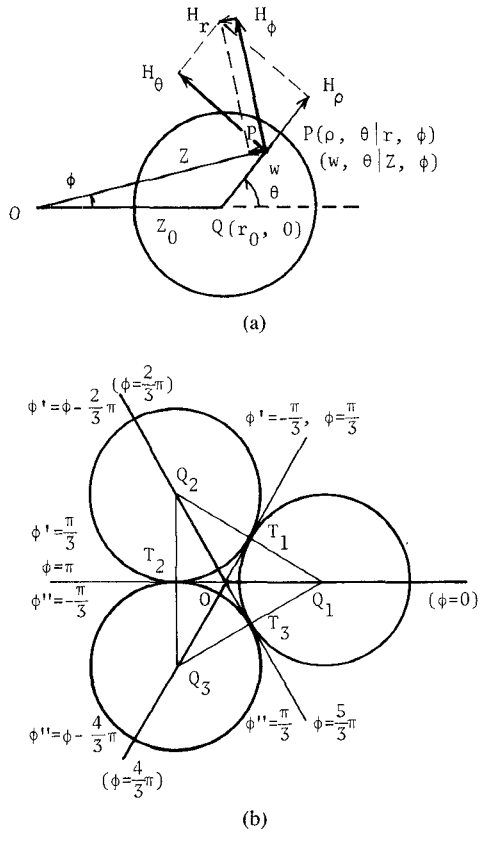

Fig. 2. (a) Relationship of radial and azimuthal components of the magnetic field in two coordinate systems (ρ, θ) and (r, ϕ), and (b) geometrical location of the TDC resonator.

$$E_z(\rho, \theta) = \sum_{\nu=-\infty}^{\infty} a_\nu J_\nu(k\rho) e^{-j\nu\theta}, \quad \rho \leq a, \tag{7}$$

$$H_\rho = +j \left[\frac{1}{\rho} \frac{\partial E_z}{\partial \theta} + j\bar{\kappa} \frac{\partial E_z}{\partial \rho} \right] \Big/ \omega\mu_0\mu_e, \tag{8}$$

$$H_\theta = -j \left[\frac{\partial E_z}{\partial \rho} - j\bar{\kappa} \frac{1}{\rho} \frac{\partial E_z}{\partial \theta} \right] \Big/ \omega\mu_0\mu_e, \tag{9}$$

where $k = \omega\sqrt{\epsilon_0\mu_0\epsilon_e\mu_e}$, $\mu_e = \mu(1 - \bar{\kappa}^2)$, $\bar{\kappa} = \kappa/\mu$, and specific permittivity and permeability of the magnetized ferrite are denoted by ϵ_e and

$$\hat{\mu} = \begin{pmatrix} \mu, & j\kappa, & 0 \\ -j\kappa, & \mu, & 0 \\ 0, & 0, & 1 \end{pmatrix},$$

respectively.

After we change a variable ρ for w, the electric field given by (7) is formulated in circular harmonic expansion as

$$E_{z+}(Z, \phi) = \sum_\nu a_\nu \sum_m J_{\nu+m}(Z) J_m(Z_0) e^{-j(\nu+m)\phi}, \tag{10}$$

$$Z_{z-}(Z, \phi) = \sum_\nu a_\nu \sum_m J_{\nu+m}(Z) J_m(Z_0) e^{-j(\nu+m)\phi}, \tag{11}$$

by using (2) and (A1). Σ_ν, and Σ_m, respectively, denote $\Sigma_{\nu=-\infty}^{\infty}$ and $\Sigma_{m=-\infty}^{\infty}$.

Meanwhile, the magnetic field which decomposes into H_r and H_ϕ can be transformed from H_ρ and H_θ as shown in Fig. 2(a), according to the relations

$$\begin{cases} H_r = H_\rho \cos\psi - H_\theta \sin\psi, \\ H_\phi = H_\rho \sin\psi + H_\theta \cos\psi. \end{cases} \tag{12}$$

In calculation of the magnetic field components, we utilize the following approximate relations of derivatives,

$$\begin{cases} \partial/\partial\rho = k\,\partial/\partial w, \\ \dfrac{\partial}{\partial w} = \dfrac{dZ}{dw}\dfrac{\partial}{\partial Z} + \dfrac{d\phi}{dw}\dfrac{\partial}{\partial\phi}, \\ \dfrac{\partial}{\partial\theta} = \dfrac{d\phi}{d\theta}\dfrac{\partial}{\partial\phi} = \dfrac{\partial}{\partial\phi}, \end{cases} \tag{13}$$

the latter two equations of which are derived from (5) and (2). Using (13) and substituting (8) and (9) into (12), we can obtain

$$H_r = j\frac{1}{\zeta_e}\left[A_1\frac{\partial E_z}{\partial Z} + \frac{A_2}{Z}\frac{\partial E_z}{\partial\phi} + j\bar{\kappa}\left\{A_3\frac{\partial E_z}{\partial Z} + \frac{A_4}{Z}\frac{\partial E_z}{\partial\phi}\right\}\right], \tag{14}$$

$$H_\phi = -j\frac{1}{\zeta_e}\left[A_3\frac{\partial E_z}{\partial Z} + \frac{A_4}{Z}\frac{\partial E_z}{\partial\phi} - j\bar{\kappa}\left\{A_1\frac{\partial E_z}{\partial Z} + \frac{A_2}{Z}\frac{\partial E_z}{\partial\phi}\right\}\right], \tag{15}$$

where

$$\begin{cases} \zeta_e = \sqrt{\mu_0\mu_e/\epsilon_0\epsilon_e}, \quad t = Z_0/Z, \quad x = \cos\phi, \\ y = \sin\phi, \quad A_1 = \dfrac{ty}{1-tx}, \quad A_2 = t + \dfrac{1-tx}{1-2tx+t^2}, \\ A_3 = 1, \quad A_4 = \dfrac{1-tx}{ty} - \dfrac{ty}{1-2tx+t^2}. \end{cases} \tag{16}$$

Thus we can derive the EM fields of the first disk positioned at $\phi = 0$ from (10), (14), and (15). Further, if we take, in place of ϕ in (10), (14), (15) and (16), $\phi' = \phi - 2\pi/3$ for the second disk, and $\phi'' = \phi - 4\pi/3$ for the third disk, we can also obtain the respective EM fields in the disks positioned at $\phi = 2\pi/3$ and $4\pi/3$.

B. Continuity Condition of The E Field in a TDC Resonator

A TDC resonator is actually a juncture of three circular disks, and they contact with each other at the distance of $r = r_0/2$ and at the angles of $\phi = \pi/3$, π and $5\pi/3$ as indicated by T_1, T_2 and T_3 in Fig. 2(b). We assume that when the juncture makes totally a unique resonator, then the E field may satisfy the continuity relation at each contact point. It gives, therefore,

$$\begin{cases} E_{z\mathrm{I}}\left(Z_1, \dfrac{\pi}{3}\right) = E_{z\mathrm{II}}\left(Z_1, -\dfrac{\pi}{3}\right), \; Z_1 = kr_0/2, \\ E_{z\mathrm{II}}\left(Z_1, \dfrac{\pi}{3}\right) = E_{z\mathrm{III}}\left(Z_1, -\dfrac{\pi}{3}\right), \\ E_{z\mathrm{III}}\left(Z_1, \dfrac{\pi}{3}\right) = E_{z\mathrm{I}}\left(Z_1, -\dfrac{\pi}{3}\right), \end{cases} \tag{17}$$

where suffices I, II and III denote three disks positioned at $r = r_0/2$ with $\phi = 0$, $2\pi/3$ and $4\pi/3$, respectively. Algebraic manipulation of (17), after substitution of (10) or (11), leads to the equality of those amplitudes

$$a_{\mathrm{I}} = a_{\mathrm{II}} = a_{\mathrm{III}}. \tag{18}$$

In calculation of the EM fields in a TDC resonator, (18) affirms to take equal amplitudes of constituent EM fields of three disks, but it does not tell whether an amplitude of each field contains a phase term of multiple of $2\pi/3$ or not.

C. Synthesis of The EM Fields in a Tridisk Juncture

The synthetic electric field of the zero phase juncture, in which each disk is assumed to take mutually the same phase among the three disks, is formulated by zero-phase-summation transformation of the constituent E fields as

$$E_z^{(0)} = \tfrac{1}{3}[E_{z\mathrm{I}}(\phi) + E_{z\mathrm{II}}(\phi') + E_{z\mathrm{III}}(\phi'')], \tag{19}$$

where $-\pi/3 \le \phi \le \pi/3$, $\phi' = \phi - 2\pi/3$, and $\phi'' = \phi - 4\pi/3$. Substituting (10) and other relevant E fields converted for ϕ' and ϕ'' into (19), we obtain

$$E_z^{(0)} = \tfrac{1}{3}\sum_\nu a_\nu\left[\sum_m J_{\nu+m}(Z)J_m(Z_0)e^{-j(\nu+m)\phi} \cdot \{1 + 2\cos(\nu+m)\beta\}\right], \tag{20}$$

where $\beta = 2\pi/3$. If an integer $(\nu + m)$ satisfies the relation

$$\begin{aligned} &1 + 2\cos(\nu+m)\beta \\ &\quad = 3, \quad \text{for } \nu + m = 3l,\ l = 0, \pm1, \pm2, \cdots, \\ &\quad = 0, \quad \text{for } \nu + m \neq 3l, \end{aligned} \tag{21}$$

only $3l$th order terms survive and others vanish. Accordingly, using the relation [7]

$$\sum_m J_m(Z_0) = 1, \tag{22}$$

and collecting all of 3-th order terms, we can get for the synthetic E field of orders $3l = 0, \pm3, \pm6, \cdots$,

$$E_{z+}^{(0)} = \sum_{3l} a_{3l}J_{3l}(Z)e^{-j3l\phi}. \tag{23}$$

Similarly, we can derive another expression, using (11),

$$E_{z-}^{(0)} = \sum_{3l} a_{3l}J_{3l}(Z)e^{-j3l\phi}. \tag{24}$$

We calculate the synthetic magnetic field, next. If we

substitute (10) into (12), the radial and azimuthal components of the synthetic H field are formulated in the same way as (19). We have consequently

$$H_{r+}^{(0)} = +j\frac{1}{\zeta_e}\sum_{\nu} a_\nu \sum_m \left[A_{\nu m}^{(0)} J'_{\nu+m}(Z) - j\frac{(\nu+m)}{Z} B_{\nu m}^{(0)} J_{\nu+m}(Z) + j\bar{\kappa}\left\{ C_{\nu m}^{(0)} J'_{\nu+m}(Z) - j\frac{(\nu+m)}{Z} D_{\nu m}^{(0)} J_{\nu+m}(Z)\right\}\right] J_m(Z_0) e^{-j(\nu+m)\phi}, \tag{25}$$

$$H_{\phi+}^{(0)} = -j\frac{1}{\zeta_e}\sum_{\nu} a_\nu \sum_m \left[C_{\nu m}^{(0)} J'_{\nu+m}(Z) - j\frac{(\nu+m)}{Z} D_{\nu m}^{(0)} J_{\nu+m}(Z) - j\bar{\kappa}\left\{ A_{\nu m}^{(0)} J'_{\nu+m}(Z) - j\frac{(\nu+m)}{Z} B_{\nu m}^{(0)} J_{\nu+m}(Z)\right\}\right] J_m(Z_0) e^{-j(\nu+m)\phi}, \tag{26}$$

where

$$\begin{cases} A_{\nu m}^{(0)} = \frac{1}{3}[A_1(\phi) + A_1'(\phi')e^{j(\nu+m)\beta} + A_1''(\phi'')e^{j2(\nu+m)\beta}], \\ B_{\nu m}^{(0)} = \frac{1}{3}[A_2(\phi) + A_2'(\phi')e^{j(\nu+m)\beta} + A_2''(\phi'')e^{j2(\nu+m)\beta}], \\ C_{\nu m}^{(0)} = \frac{1}{3}[1 + e^{j(\nu+m)\beta} + e^{j2(\nu+m)\beta}], \\ D_{\nu m}^{(0)} = \frac{1}{3}[A_4(\phi) + A_4'(\phi')e^{j(\nu+m)\beta} + A_4''(\phi'')e^{j2(\nu+m)\beta}]. \end{cases} \tag{27}$$

A_1', A_1'', A_2', A_2'' and others in (27) indicate the quantities of A_1, A_2 and others all of which are replaced by $\phi' = \phi - \beta$ and $\phi'' = \phi - 2\beta$, respectively.

As to all the integers $\nu + m$, if (21) satisfies, we can prove that

$$A_{\nu m}^{(0)} = A, \quad B_{\nu m}^{(0)} = B, \quad C_{\nu m}^{(0)} = 1, \quad D_{\nu m}^{(0)} = D, \tag{28}$$

where

$$\begin{cases} A = \dfrac{t^3 \sin 3\phi}{4 - 3t^2 + t^3 \cos 3\phi}, \\ B = t + \dfrac{1 - t^3 \cos 3\phi}{1 - 2t^3 \cos 3\phi + t^6}, \\ D = \dfrac{1 - t\cos 3\phi}{t \sin 3\phi} - \dfrac{t^3 \sin 3\phi}{1 - 2t^3 \cos 3\phi + t^6}. \end{cases} \tag{29}$$

Subsequently, applying (22), we find the magnetic field components for modes of orders $3l = 0, \pm 3, \pm 6, \cdots$,

$$H_{r+}^{(0)} = +j\frac{1}{\zeta_e}\sum_{3l} a_{3l}\left[AJ'_{3l}(Z) - j\frac{3l}{Z} BJ_{3l}(Z) + j\bar{\kappa}\left\{ J'_{3l}(Z) - j\frac{3l}{Z} DJ_{3l}(Z)\right\}\right] e^{-j3l\phi}, \tag{30}$$

$$H_{\phi+}^{(0)} = -j\frac{1}{\zeta_e}\sum_{3l} a_{3l}\left[J'_{3l}(Z) - j\frac{3l}{Z} DJ_{3l}(Z) - j\bar{\kappa}\left\{ AJ'_{3l}(Z) - j\frac{3l}{Z} BJ_{3l}(Z)\right\}\right] e^{-j3l\phi}. \tag{31}$$

The synthetic EM fields in both cases of positive and negative phase junctures are calculated in Appendix B. The results obtained for both cases are the same as those for the above case of the zero-phase juncture.

D. The EM fields in The TDC Resonator

Deducing the synthetic EM field expressions for the above three cases, we can present the EM fields for all modes $n = 3l - 1$, $3l$ and $3l + 1$ ($l = 0, 1, 2, \cdots$) as

$$E_z = \sum_n a_n J_n(Z) e^{-jn\phi}, \tag{32}$$

$$H_r = +j\frac{1}{\zeta_e}\sum_n a_n\left[AJ'_n(Z) - j\frac{n}{Z} BJ_n(Z) + j\bar{\kappa}\left\{ J'_n(Z) - j\frac{n}{Z} DJ_n(Z)\right\}\right] e^{-jn\phi}, \tag{33}$$

$$H_\phi = -j\frac{1}{\zeta_e}\sum_n a_n\left[J'_n(Z) - j\frac{n}{Z} DJ_n(Z) - j\bar{\kappa}\left\{ AJ'_n(Z) - j\frac{n}{Z} BJ_n(Z)\right\}\right] e^{-jn\phi}. \tag{34}$$

The synthetic magnetic field components H_r and H_ϕ include A, B and D, which are shown in Fig. 3. All of A, B and D have a periodicity of $2\pi/3$ in ϕ, and in particular, A and D vanish at $\phi = 0$ and a multiple of $2\pi/3$. Contrarily, B may have a larger value than unity. From the practical point of view, the input port to the resonator is ordinarily attached at $\phi = 0$ or a multiple of $2\pi/3$ on the periphery of a disk in a TDC resonator, and consequently we choose such particular angles that A and D vanish.

E. Eigenvalues of Resonant Modes

Assume that the TDC resonator is devised with the requirement for $A = D = 0$. Resonant modes of the TDC resonator are defined to satisfy the magnetically short-circuited edge at an assumed periphery of radius r_2, and therefore the equation, $H_\phi(r_2) = 0$, gives the characteristic equations of resonant modes. As for the modes of $\pm n$th orders, we have from (34)

$$J'_n(Z_2) \mp \bar{\kappa}'\frac{n}{Z_2} J_n(Z_2) = 0, \tag{35}$$

$$Z_2 = kr_2 = ka(1 + \Delta), \qquad \bar{\kappa}' = \bar{\kappa} B_0. \tag{36}$$

$a\Delta$ is the increment of radius that is adjusted to the experimental result. The anisotropic splitting factor of the

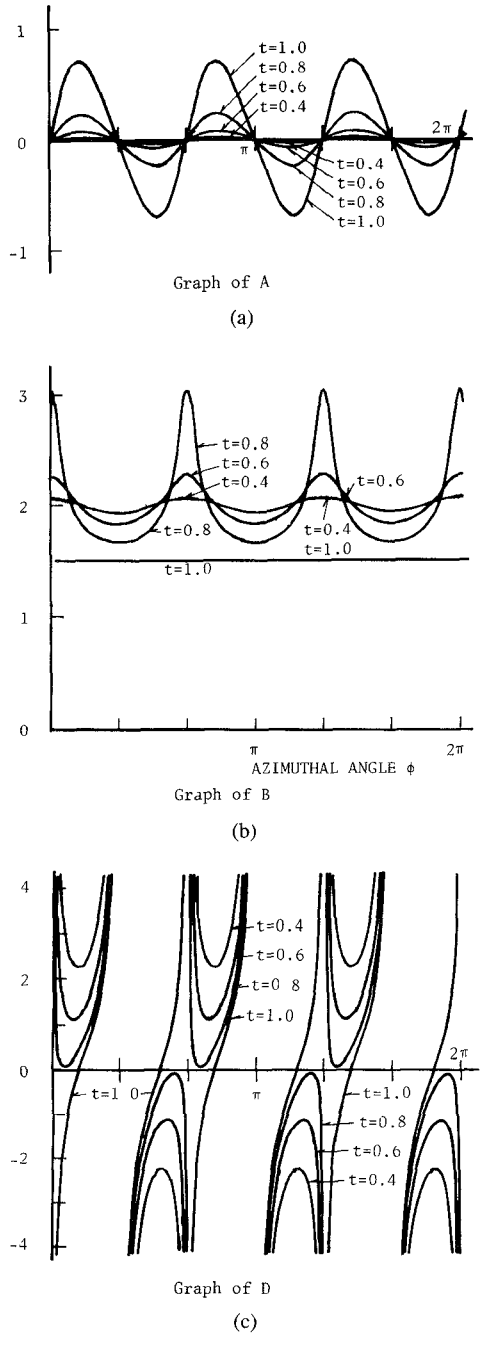

Fig. 3. Graphs of A (a), B (b) and D (c) as functions of t (= r_0/r) and ϕ.

juncture $\bar{\kappa}'$ is devised to describe the bound region of $\bar{\kappa}$.

Determination of $1 + \Delta$ and B_0 is made as follows. With the experimental mode chart as shown in Fig. 7, we can find out degenerate resonant frequencies of the disk and TDC resonators at $f_{dg\text{disk}} = 1.81$ GHz and $f_{dg\text{TDC}} = 1.17$ GHz, respectively, which can be read regarding pair modal curves $\nu = \pm 1$ and $n = \pm 1$, by exterpolation, at the extremity of biasing magnetic field. The degenerate eigenvalue of the disk that is given by $J_1'(ka) = 0$ is $(ka)_{\text{disk}} = 1.84$, and also that of the TDC resonator $[ka]_{\text{TDC}}(1 + \Delta) = 1.84$. As we can suppose a linear dependence of eigenvalue on frequency, we formulate the relationship between the degenerate resonant frequencies and eigen-

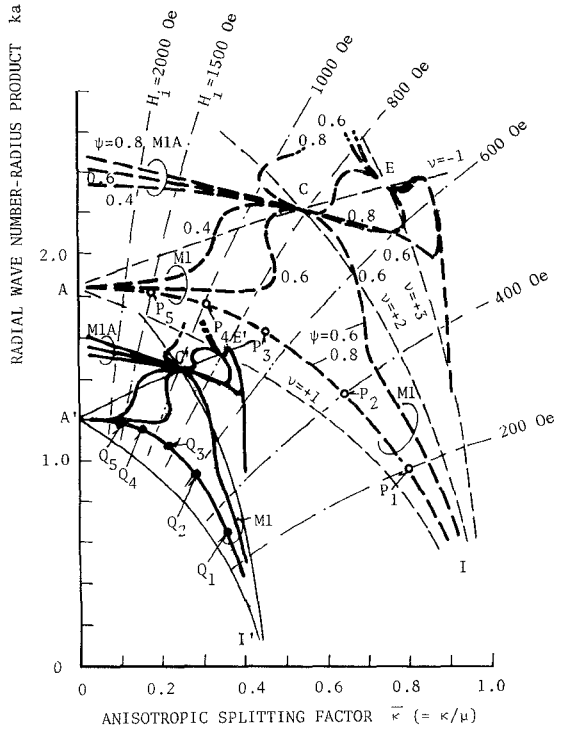

Fig. 4. Comparison of the first circulation conditional curves of the monodisk and TDC Y junctions superimposed on the respective resonant mode curves. Broken and solid lines, respectively, denote the related curves of the monodisk and TDC resonators and their applied Y junctions. M1 and M1A denote mode 1 and mode 1A among circulating modes. The ordinate ka is commonly utilized. ψ is half the stripline coupling angle.

values as

$$\frac{(ka)_{\text{disk}}}{[ka]_{\text{TDC}}} = \frac{f_{dg\text{disk}}}{f_{dg\text{TDC}}} = \frac{1.81\ \text{GHz}}{1.17\ \text{GHz}} = 1 + \Delta. \qquad (37)$$

Then we have, for the case of a disk scraped by 1 mm,

$$1 + \Delta = 1.547, \quad [ka]_{\text{TDC}} = 1.189, \quad r_0 = 10.4\ \text{mm},$$

$$r_2 = a(1 + \Delta) = 15.47\ \text{mm}, \quad t = r_0/r_2 = 0.67,$$

and we find from the graph of B in Fig. 3(b)

$$B_0 = 2.22 \quad \text{and} \quad \bar{\kappa}_{\max} = 0.45\ (= 1/B_0).$$

Consequently the resonant mode curves of $n = \pm 1$ are shifted downwards to $[ka] = 1.19$, and bound in the region from $\bar{\kappa} = 0$ to $\bar{\kappa}_{\max} = 0.45$. The resonant mode curves of $n = \pm 1$ in addition to $\nu = \pm 1$ will be shown in Fig. 4.

III. Two Conditional Curves of Perfect Y Circulation and Circulation Adjustments

We introduce two conditional equations of perfect Y circulation which are given in Appendix C. Numerical computation of the first and second conditional equations, (A11) and (A12), is carried out. Regarding the second conditional equation, the ever-made computed results which were disclosed elsewhere [3] were obviously difficult to understand. Solutions of the second conditional equation should, as a matter of course, give necessary and

understandable base of knowledge to get circulation adjustments. In this paper we choose a graphical method more feasible for understanding the way of impedance matching. We rewrite (A12) as for the coupled stripline characteristic impedance Z_d

$$Z_d = Z_{yeq}, \tag{38}$$

where

$$Z_{yeq} = \sqrt{3}\,\frac{\psi}{\pi}\,Z_e\,\frac{2h_1h_2 - h_0(h_1 + h_2)}{(h_1 - h_2)}, \tag{39}$$

$$Z_e \simeq \frac{\zeta_e}{4}\log\left(\frac{W + D}{W + t}\right), \quad W \simeq 2\psi r_2, \tag{40}$$

ζ_e is the intrinsic wave impedance of the ferrite, W the center conductor width of stripline, t its thickness, D the spacing between two earthed conductor, and ψ half the coupling angle of stripline. (38) means that Z_d the coupled stripline impedance should match Z_{yeq} the equivalent input impedance of the stripline Y junction. The stripline characteristic impedance outside the ferrite which is required for impedance matching is approximately given by

$$Z_d \simeq \frac{\zeta_d}{4}\log\left(\frac{W' + D}{W' + t}\right), \tag{41}$$

where ζ_d is $\sqrt{\mu_0/\epsilon_0\epsilon_d}$ the intrinsic wave impedance of the dielectric used, W' its width, and both D and t are the same as those said above.

The computed results of the first and second conditional equations are shown in Figs. 4 and 5, both being superimposed for the TDC and monodisk resonators and the respective Y junctions. In Fig. 4, resonant mode curves of the two resonators are drawn to distinguish circulating mode curves of the lowest orders, with several loci of constant internal magnetic field intensity H_i additionally drawn upon along with the common ordinate ka. The relationship of resonant mode curves against circulating mode curves of the TDC Y junction (solid lines) is apparently similar to that of the monodisk Y junction (broken lines). Though the modal curves of two kinds of the TDC Y junction lie in the region of lower ka and less $\bar{\kappa}$ values, correspondences of the relationships of resonant and circulating modes between the two Y junctions are clearly discerned if one compares A, C, E and I with A', C', E' and I'.

Fig. 5 shows the relationship of the equivalent input impedance Z_{yeq} versus $\bar{\kappa}$ for the lowest order modes of the TDC and monodisk Y junctions. Mode 1 has the bottom flatness of Z_{yeq} at about 20 Ω for both Y junctions.

To examine more presicely the two conditional curves in Figs. 4 and 5, we choose some operating points on a circulating mode curve that may be definitely fixed by intersections with loci of given values of H_i. With H_i stepwise increasing from H_i = 200 Oe, we can fix operating

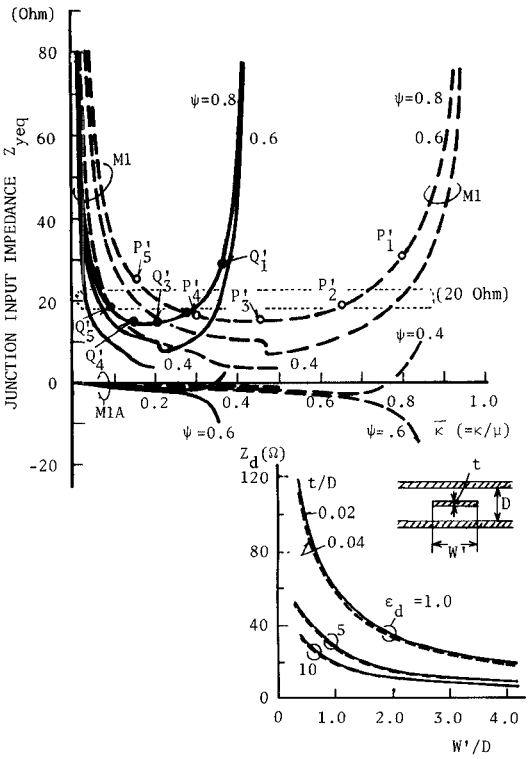

Fig. 5. Comparison of the second circulation conditional curves of the monodisk (broken lines) and TDC (solid lines) Y junctions. Mode numbers M1 and M1A correspond to those usages in Fig. 4. (20 Ω) denotes a possible region of 20 Ω in circulation adjustment for the series operation of mode 1. Indented is the Z_d versus W'/D relationship of stripline.

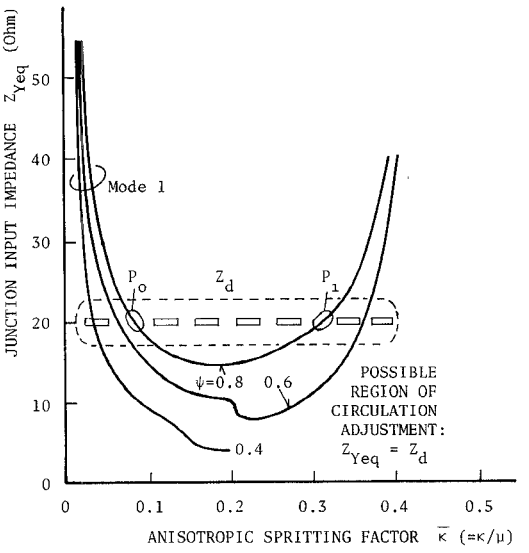

Fig. 6. Illustration of the graphical method of circulation adjustments for the series operation of mode 1 in the bottom flatness of Z_{yeq}.

points P_1, P_2, · · · on the mode 1 curve of $\psi = 0.8$ of the monodisk Y junction, and likewise, Q_1, Q_2, · · · on the mode 1 curve of the TDC Y junction. We can transfer all of these operating points in Fig. 4 onto impedance points of Z_{yeq} on the corresponding mode curves in Fig. 5. The latter points are distinguished with primes on letters as P_1', P_2' and so on.

We can find out that P_2', $\cdots$ P_5' and Q_2', $\cdots$ Q_5' are on the flatness in the vicinity of $Z_{yeq} = 20\ \Omega$. These are operating points of mode 1 circulation that is magnetically tunable.

Circulation at each operating point on the mode 1 curve is possible to satisfy the second condition to get perfect operation if its operating value of Z_{yeq} on such bottom flatness matches a coupled stripline impedance Z_d. This is graphically exemplified in Fig. 6. We must choose the most probable value of Z_d (thick broken line), in order to coincide sufficiently with the average value of Z_{yeq} from P_i to P_o, which is shown surrounded by a broken line. Stripline impedance Z_d is practically adjusted by choosing stripline width W' and other parameters, which is shown indented in Fig. 5.

IV. Experiments and Discussions

In the experiments, the TDC resonator used had such specifications that the diameter of a disk was 20 mm, its thickness 2.5 mm, scraped depth 1.0 mm, the diameter of the center conductor for the resonator 42 mm, the saturation magnetization of the ferrite $4\pi M_s = 950$ Gauss, and its permittivity $\epsilon_e = 14.5$, and the Y junction had such dimensions that the center-conductor of coupled stripline was 18 mm in width, its thickness 0.2 mm, and the spacing $D = 5.5$ mm. Stripline tapers were used.

To examine experimentally the resonant modes in the TDC resonator, a mode chart was obtained on which measured resonant frequencies were plotted against biasing magnetic field intensity as shown in Fig. 7. There are two mode charts superimposed so as to compare between mondisk and TDC resonators. It is recognized that the lowest resonant modes of $n = \pm 1$ in the TDC resonator appeared far below those of $\nu = \pm 1$ in the monodisk resonator.

An example of the magnetically tunable operation is shown in Fig. 8. As the biasing magnetic field intensified, an incessant constituent operation having a narrow frequency band of less than 100 MHz moved toward higher frequencies. It covered an operating frequency band from 0.4 to 1.1 GHz. The constituent operation had insertion losses of less than 1.5 dB, gradually decreasing to 0.3 dB in higher frequencies, and isolation of more than 25 dB.

Granting that an operating point of a circulator agrees experimentally to a frequency of maximum isolation in a given biasing magnetic field intensity, operating points of the magnetically tunable operation can be measured. Measured operating frequencies are plotted in the mode chart as shown in Fig. 7. We find out that all the operating points lie between two resonant mode curves of $n = +1$ and -1. This proves that mode 1 circulation plays an essential role in this operation.

The impedance matching as circulation adjustment of the Y junction at several operating points were examined by measuring VSWR at the input port, with other ports being matched. The measured VSWR versus frequency

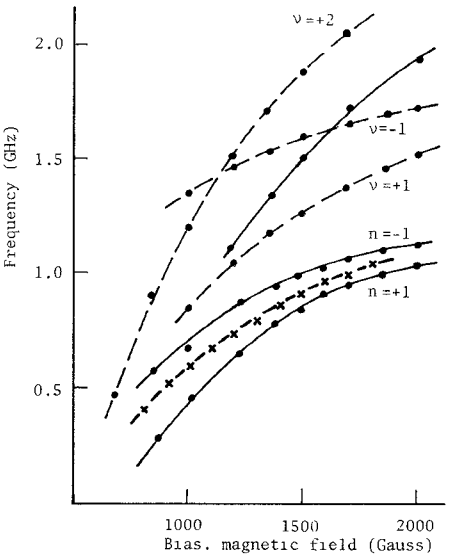

Fig. 7. Comparison of resonan modes of TDC resonator (solid lines) and mondisk resonator (broken lines). Small x's indicate operating points of the magnetically tunable operation.

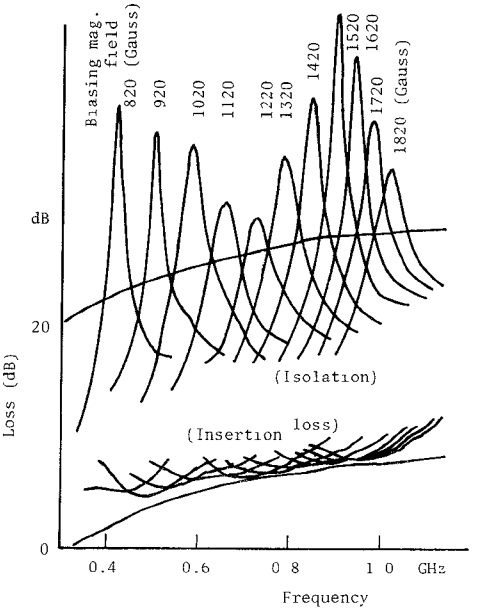

Fig. 8. Example of the magnetically tunable operation of the stripline Y junction with the TDC resonators.

relationship is shown in Fig. 9. The VSWR minima at 0.5 and 0.9 GHz are considered to correspond to better circulation adjustments which are mentioned above with respect to the intersection between the Z_d level line and the bottom flatness of Z_{yeq} as shown in Fig. 6, and a hump in the intermediate may be caused to the slight mismatching in the middle region.

Throughout the present experiment, ferrite disks which were partially scraped to tightly couple with each other were utilized. The role that they played has not been mentioned. It is, however, worthwhile to add to say that the insertion losses of the circulator were appreciably decreased with such scraping.

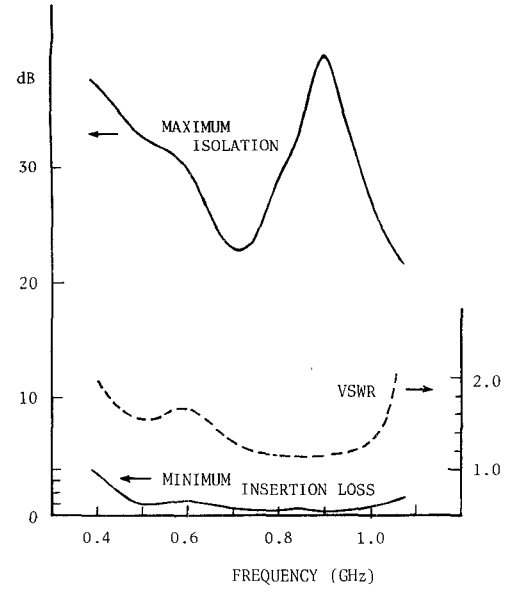

Fig. 9. Measured VSWR versus frequency characteristics of the magnetically tunable operation. Both maximum isolation and minimum insertion loss characteristics are drawn for comparison.

V. Conclusion

In this paper we dealt with a TDC resonator and its applied stripline Y circulator, and we demonstrated theoretically and experimentally that the magnetically tunable operation was performed with the mode 1 operation of perfect Y circulation.

In theoretical analysis, we discussed that (1) the EM fields in the TDC resonator were synthesized from the respective EM fields of constituent monodisk resonators located at $\phi = 0, 2\pi/3$ and $4\pi/3$ and they included structural coefficients A, B and D; and only a special case that $A = D = 0$ was adopted; (2) the resonant modes of the TDC resonator was effectuated by $B_0(\kappa/\mu)$ the anisotropic splitting factor, and the resonant modes existed in the region of lower ka and less κ/μ values in comparison with those of a monodisk resonator; (3) the circulating mode curves of the first and second conditions were examined with respect to the mode 1 circulation, with emphasis on circulation adjustments, and the mode 1 circulation had advantage in achieving circulation adjustments since its input junction impedance Z_{yeq} took a bottom flatness near 20 Ω.

In the experiments, we demonstrated that (1) resonant modes of the TDC resonator existed in the lower frequency region; (2) the magnetically tunable operation was identified as the mode 1 circulation; (3) the VSWR versus frequency characteristics showed the general feature of the well achieved impedance matching over the bottom flatness of Z_{yeq}.

Consistent theory of the TDC resonator will appear in near future.

Finally the authors express their thanks to graduates Tadashi Arai and Kimiyoshi Motogi for their endeavors.

Appendix

A. Addition Theorem of Bessel Functions [7]

$$e^{\nu j\psi}J_\nu(w) = \sum_{m=-\infty}^{\infty} J_{\nu+m}(Z)J_m(Z_0)e^{jm\phi},$$

$$e^{-\nu j\psi}J_\nu(w) = \sum_{m=-\infty}^{\infty} J_{\nu+m}(Z)J_m(Z_0)e^{-jm\phi}. \quad \text{(A1)}$$

B. Calculation of The EM Fields in The Cases of The Positive and Negative Junctures

The synthetic E field in the positive phase juncture is formulated as

$$E_z^{(+)} = \tfrac{1}{3}[E_{zI}(\phi) + E_{zII}(\phi')e^{-j\beta} + E_{zIII}(\phi'')e^{-j2\beta}]. \quad \text{(A2)}$$

Substituting (10) and other relevant fields converted for ϕ' and ϕ'' into (A2), applying the following requirement for integers $(\nu + m - 1)$

$$\begin{aligned} 1 + 2\cos(\nu + m - 1)\beta &= 3, \quad \text{for } \nu + m = 3l + 1 \\ &\quad (= \cdots -2, 1, 4, 7, \cdots), \\ &= 0, \quad \text{otherwise,} \end{aligned} \quad \text{(A3)}$$

and using (22), we find for the E field of modes of orders $3l + 1$

$$E_z^{(+)} = \sum_{3l+1} a_{3l+1}J_{3l+1}(Z)e^{-j(3l+1)\phi}. \quad \text{(A4)}$$

The radial and azimuthal components of the synthetic H field, $H_r^{(+)}$ and $H_\phi^{(+)}$, are formulated in the same way as (25) and (26), following (A2), and the four structural coefficients are described, following

$$\begin{aligned} A_{\nu m}^{(+)} = \tfrac{1}{3}[&A_1(\phi) + A_1'(\phi')e^{j(\nu+m-1)\beta} \\ &+ A_1''(\phi'')e^{j2(\nu+m-1)\beta}]. \end{aligned} \quad \text{(A5)}$$

If (A3) satisfies as to all integers $(\nu + m - 1) = 3l$, we can prove that

$$A_{\nu m}^{(+)} = A, \quad B_{\nu m}^{(+)} = B, \quad C_{\nu m}^{(+)} = 1, \quad D_{\nu m}^{(+)} = D. \quad \text{(A6)}$$

Consequently, as to the modes of orders $\nu + m = 3l + 1$, we also get the same expressions of the magnetic field as we have in (30) and (31).

As for the negative phase juncture, the synthetic E field is formulated as

$$E_z^{(-)} = \tfrac{1}{3}[E_{zI}(\phi) + E_{zII}(\phi')e^{j\beta} + E_{zIII}(\phi'')e^{j2\beta}]. \quad \text{(A7)}$$

If for integers $(\nu + m + 1)$ it satisfies the relation

$$\begin{aligned} 1 + 2\cos(\nu + m + 1)\beta \\ = 3, \quad \text{for } \nu + m = 3l - 1 (= \cdots -1, 2, 5, \cdots), \\ = 0, \quad \text{otherwise,} \end{aligned} \quad \text{(A8)}$$

as we have shown above, the radial and azimuthal components of the synthetic magnetic field, $H_r^{(-)}$ and $H_\phi^{(-)}$,

are calculated for all modes of orders $\nu + m = 3l + 1$, and all coefficients $A_{\nu m}^{(-)}$, $B_{\nu m}^{(-)}$, $C_{\nu m}^{(-)}$, and $D_{\nu m}^{(-)}$ are also described, following

$$A_{\nu m}^{(-)} = \tfrac{1}{3}[A_1(\phi) + A_1'(\phi')e^{j(\nu+m+1)\beta} + A_1''(\phi'')e^{j2(\nu+m+1)\beta}]. \quad \text{(A9)}$$

They are also proved to be

$$A_{\nu m}^{(-)} = A, \quad B_{\nu m}^{(-)} = B, \quad C_{\nu m}^{(-)} = 1, \quad D_{\nu m}^{(-)} = D. \quad \text{(A10)}$$

Consequently, as to the modes of orders $\nu + m = 3l - 1$, we can get the same expressions of the magnetic field components that are given in (30) and (31).

C. The First and Second Conditional Equations of Perfect Y Circulation

They are cited from [3]. The first and second conditional equations are given as follows;

$$(h_0 + h_1 + h_2)(h_0h_1 + h_1h_2 + h_2h_0) - 9h_0h_1h_2 = 0, \quad \text{(A11)}$$

$$\sqrt{3}\,\frac{\psi}{\pi}\,(Z_e/Z_d) = \frac{h_1 - h_2}{2h_1h_2 - h_0(h_1 + h_2)}, \quad \text{(A12)}$$

where

$$h_0 = \sum_{i=0}^{\infty} S(3i\psi)\,\frac{2f_{3ia}}{f_{3ia}^2 - (g_{3i} - f_{3is})^2},$$

$$h_1 = \sum_{i=-\infty}^{\infty} S\{(3i+1)\psi\}\,\frac{1}{f_{3i+1} - g_{3i+1}},$$

$$h_2 = \sum_{i=-\infty}^{\infty} S\{(3i-1)\psi\}\,\frac{1}{f_{3i-1} - g_{3i-1}},$$

and for all $n = 3i - 1, 3i, 3i + 1$,

$$f_n = J_n'(Z_2)/J_n(Z_2), \quad g_n = (\kappa/\mu)n/Z_2,$$

$$f_{na} = (f_n + f_{-n})/2, \quad f_{ns} = (f_n - f_{-n})/2,$$

ψ is half the stripline coupling angle, Z_e and Z_d are wave impedances of coupled striplines inside and outside the ferrite resonator, respectively.

REFERENCES

[1] J. B. Davies and P. Cohen, "Theoretical design of symmetrical junction stripline circulator," *IEEE Trans. Microwave Theory Tech.*, vol. MTT-11, pp. 506–512, Nov. 1963.

[2] H. Bosma, "On stripline Y-circulation at UHF," *IEEE Trans. Microwave Theory Tech.*, vol MTT-12, pp. 61–72, Jan. 1964.

[3] T. Nagao and Z. Tanaka, "Diplexer operation of stripline Y circulator: Pt. 1," *IEEE Trans. Microwave Theory Tech.*, vol. MTT-28, pp. 776–786, July 1980.

[4] T. Nagao and Z. Tanaka, "Magnetically tunable stripline Y circulator," in *1990 IEEE MTT-S Int. Microwave Symp. Dig.* CC-3, pp. 1011–1014, May 1990.

[5] E. Yamashita, S. Ozeki and K. Atsuki, "Modal analysis method for optical fibers with symmetrically distributed multiple cores," *IEEE J. Lightwave Tech.*, vol. LT-3, pp. 341–346, 1985.

[6] H. S. Huang and H. C. Hang, "Analysis of equilateral three-core fibers by circular harmonic expansion method," *IEEE J. Lightwave Tech.*, vol. LT-8, pp. 945–952, 1990.

[7] G. N. Watson, "A treatise on the Theory of Bessel Functions," 2nd ed., London: Cambridge University Press, 1966.

Tsukasa Nagao (M'72–SM'73), photograph and biography not available at the time of publication.

Zengo Tanaka, photograph and biography not available at the time of publication.